Biophysical Journal, Volume *116*

Supplemental Information

Mechanisms for Benzene Dissociation through the Excited State of T4 Lysozyme L99A Mutant

Victoria A. Feher, Jamie M. Schiffer, Daniel J. Mermelstein, Nathan Mih, Levi C.T. Pierce, J. Andrew McCammon, and Rommie E. Amaro

Supporting Material for:

Mechanisms for Benzene Dissociation through the Excited State of T4 Lysozyme L99A mutant.

Feher, V. A. [†*], Schiffer, J. M. [†], Mermelstein, D., Mih, N., Pierce, L.C.T., McCammon, J.A., Amaro, R. E.[*]

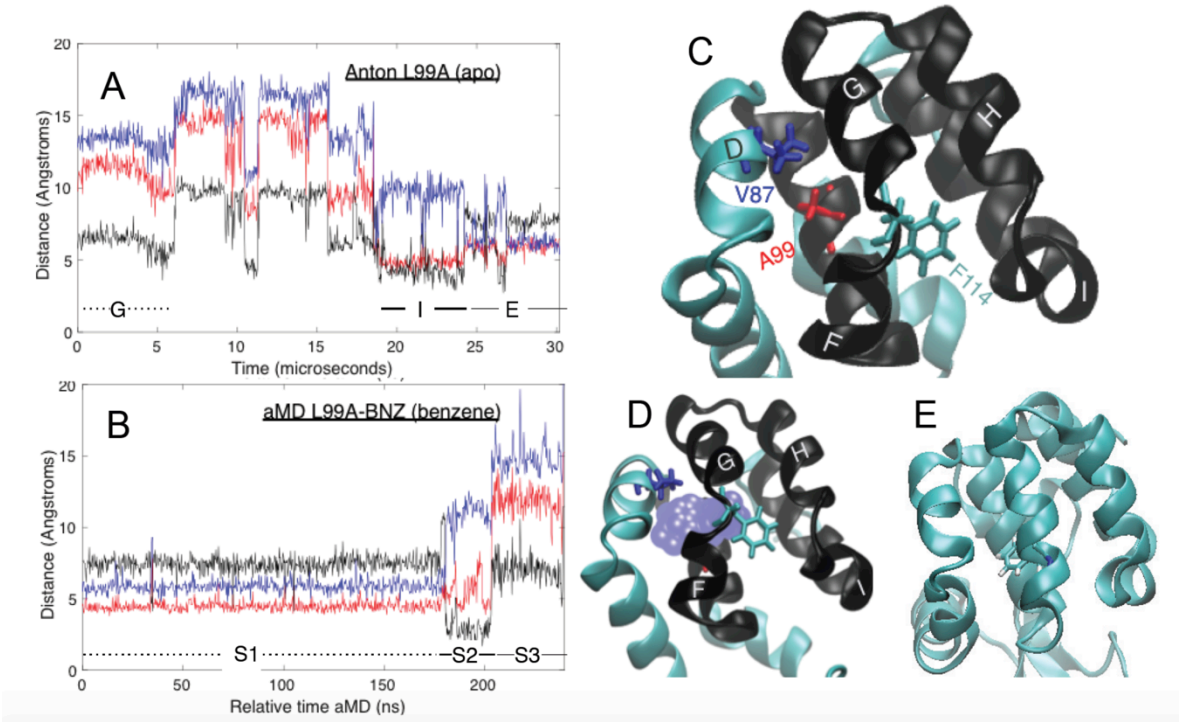

Figure S1 | Benzene egress occurs through a previously characterized transition state and excited state. (A) Previously published (1) characterization of ground to excited state transition as observed by Anton simulation for apo L99A are shown for comparison to data presented here. The the side chain of F114 is initially buried in the 4-helix bundle of the C-terminal domain and over the course of the transition moves to the cavity created by L99A mutation. Internal distances were measured between the center of mass between the aromatic ring of F114 (A) to the beta carbon of A99 (red), the beta carbon of V87 (blue), and the center of mass of the four helix bundle (black). (B) Internal distances for the center of mass of benzene to the A99 beta carbon (red), beta carbon of V87 and center of mass of the four helix bundle (black)

show benzene follows a similar path through the transition state to excited state as F114 in (A) albeit in the opposite direction. Note F114 also follows the path observed in (a) during the aMD simulation where benzene exits, with it's final position in the L99A created cavity of the excited state. Panels (C, D and E) illustrate the position of the residues used for internal distance measurement; (C) shows the locations of A99 (red), V87 (blue), F114 (cyan) and the four helix bundle (black) in the ground state, (D) illustrates the location of buried cavity relative to the 4-helix bundle (PDB: 4W51) and (E) illustrates the position of F114 when L99A samples S2 state in the aMD simulation.

Figure S2 | C-terminal domain backbone flexibility during benzene egress. Snapshots from the aMD trajectory during benzene (orange) egress demonstrate the inherent flexibility of the F and G helices in the C-terminal domain of the L99A cavity mutant, cyan, during the transition. The ground state holo crystal structure is shown for reference in gray.

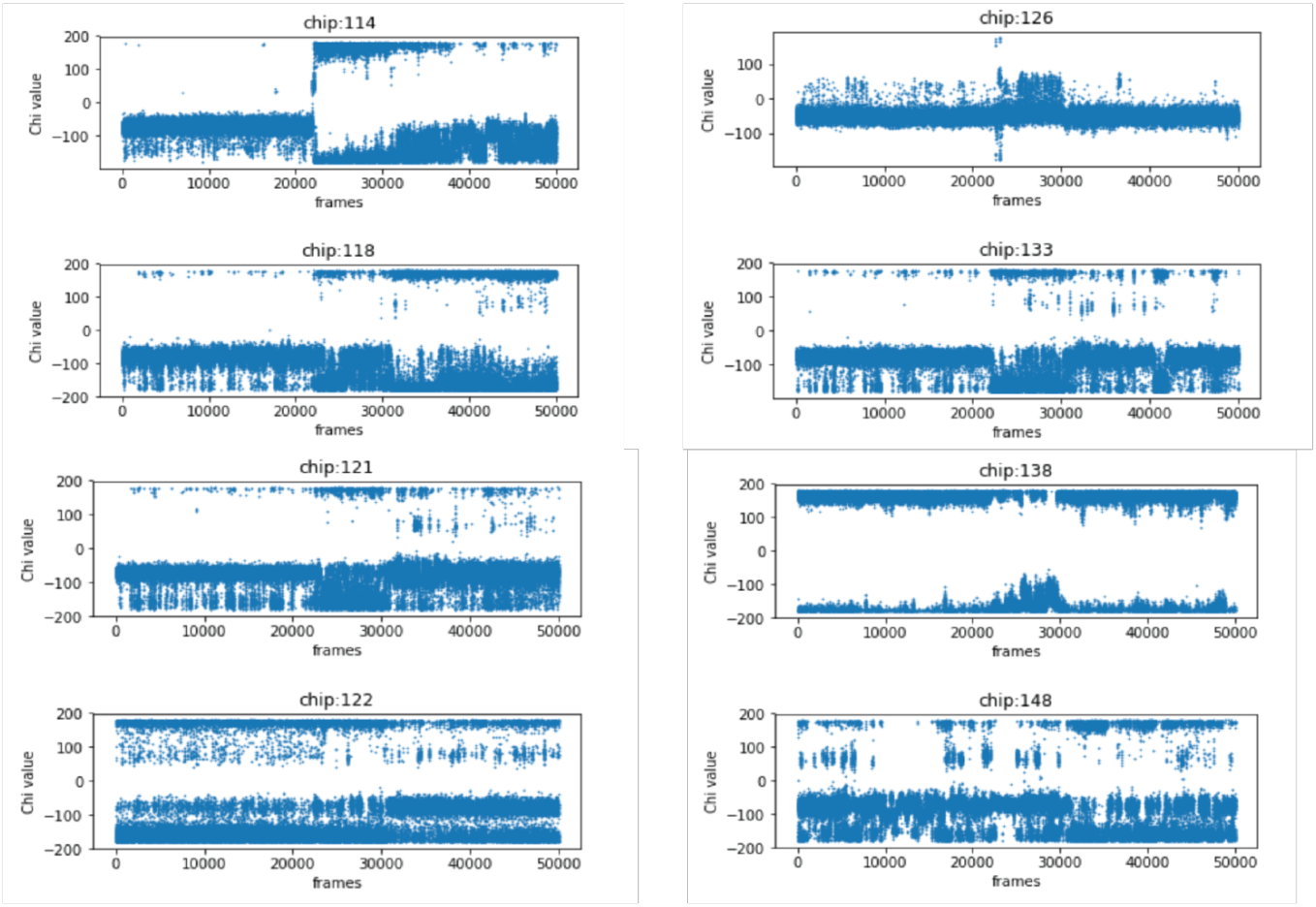

Figure S3 | Dihedral angle rotamers for buried hydrophobic residues of the C-terminal domain during holo L99A simulation where benzene egresses. An array of χ_1 rotamers are followed for residues (left to right and top to bottom 114, 126, 118, 133, 121, 138, 122, 148) are mapped over time for the aMD trajectory where benzene begins egress at time step ~25000.

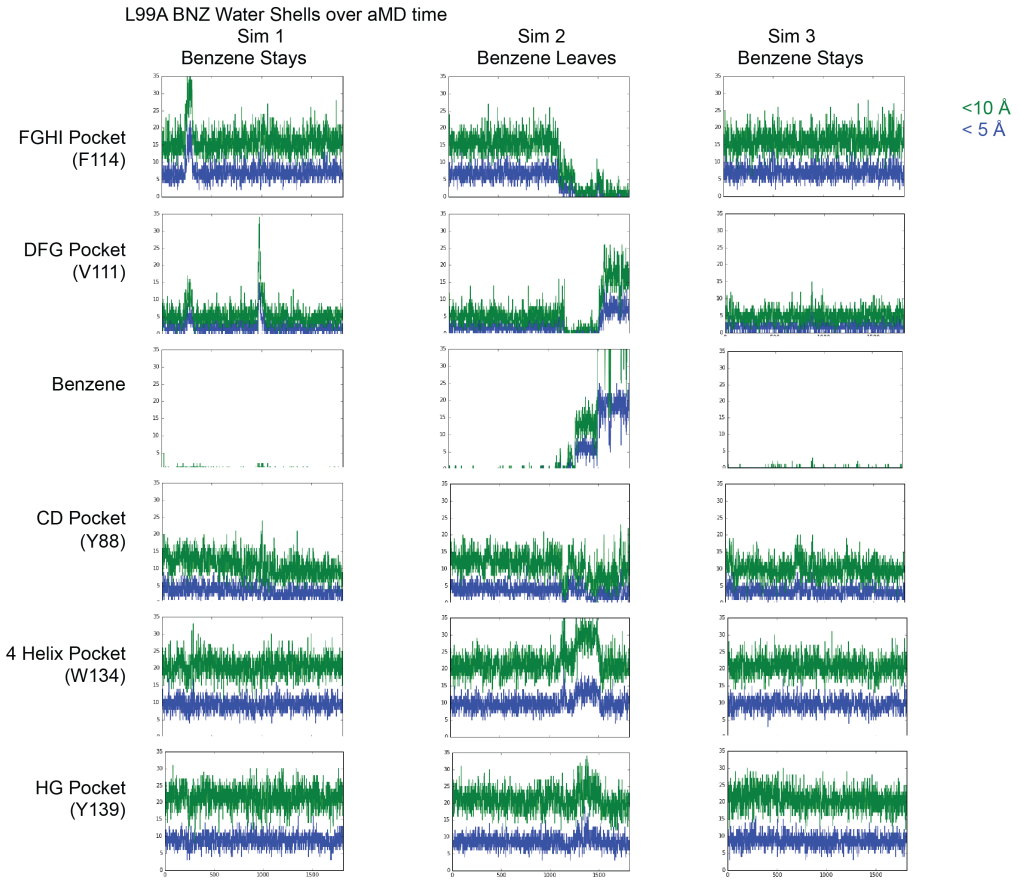

Figure S4 | Number of Waters in Watershells Around the L99A C-terminal Domain Pockets and Benzene in the Holo Simulations. Each of the three replicates of the benzene bound L99A simulations are shown in the columns above. The different pockets/benzene are shown in rows. The number of waters in the first water shell are shown in blue, while the number of waters in the second watershell are shown in green. The y-axis in all the plots spans from 0 waters to 35 waters. The x-axis shows the timestep of each replicate.

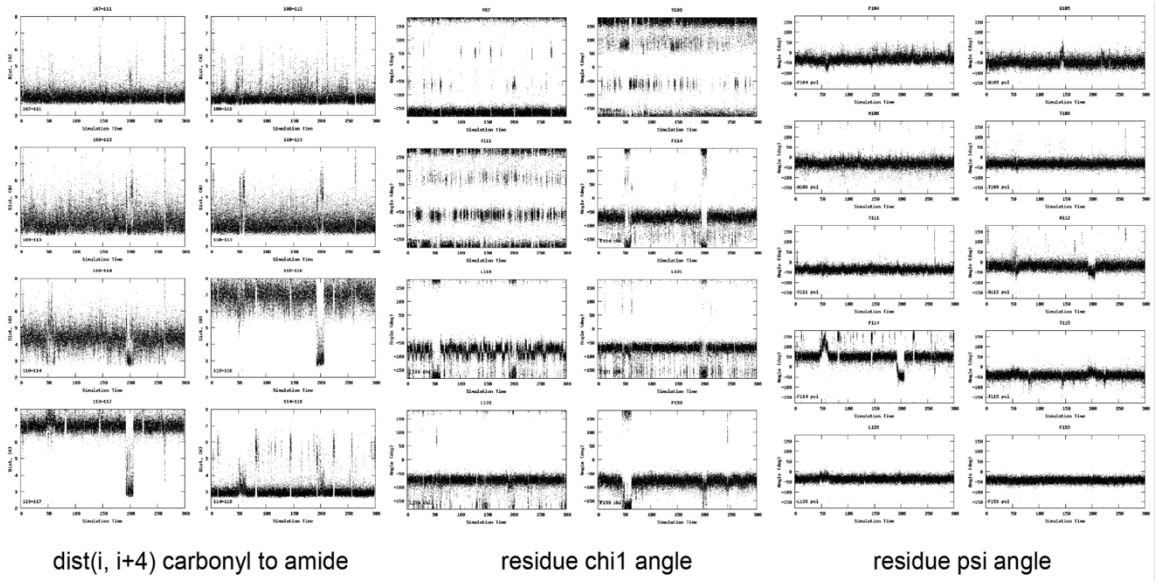

Figure S5 | Backbone hydrogen bond breakages and side chain and backbone torsion angle changes that accompany non-productive excursions from the ground state. An array of backbone hydrogen bond distances, χ_1 angle, and ψ angle changes from an aMD trajectory where benzene does not egress but exchanges between the S1 and S2 states of benzene. The difference between a productive and non-productive transition depends upon the extent of coincidence for both backbone and side chain torsion angles. In the cases where benzene moves around in the buried cavity but does not leave during our aMD trajectories (column 1, Figure 2), conformational changes are less concerted. Two instances of rotamer shifts are witness, at 3,000 aMD timesteps and at 13,000 aMD timesteps. The first non-productive excursion results from shifting of both F114 and F153 χ_1 rotamer flips, but are unaccompanied by any backbone conformational changes or motion of benzene. The second non-productive excursion results from F114 χ_1 rotamer flips as well as folding of the F and G helices into a single helix, as witnessed in the reduction

in distance between backbone nitrogen of G113 and the backbone carbonyl oxygen of S117. This second excursion is accompanied by benzene shifting to an S2-like substate. However, in this second excursion, F153 and L133 χ_1 rotamer flips do not follow the transition, and benzene returns back to its crystallographic position.

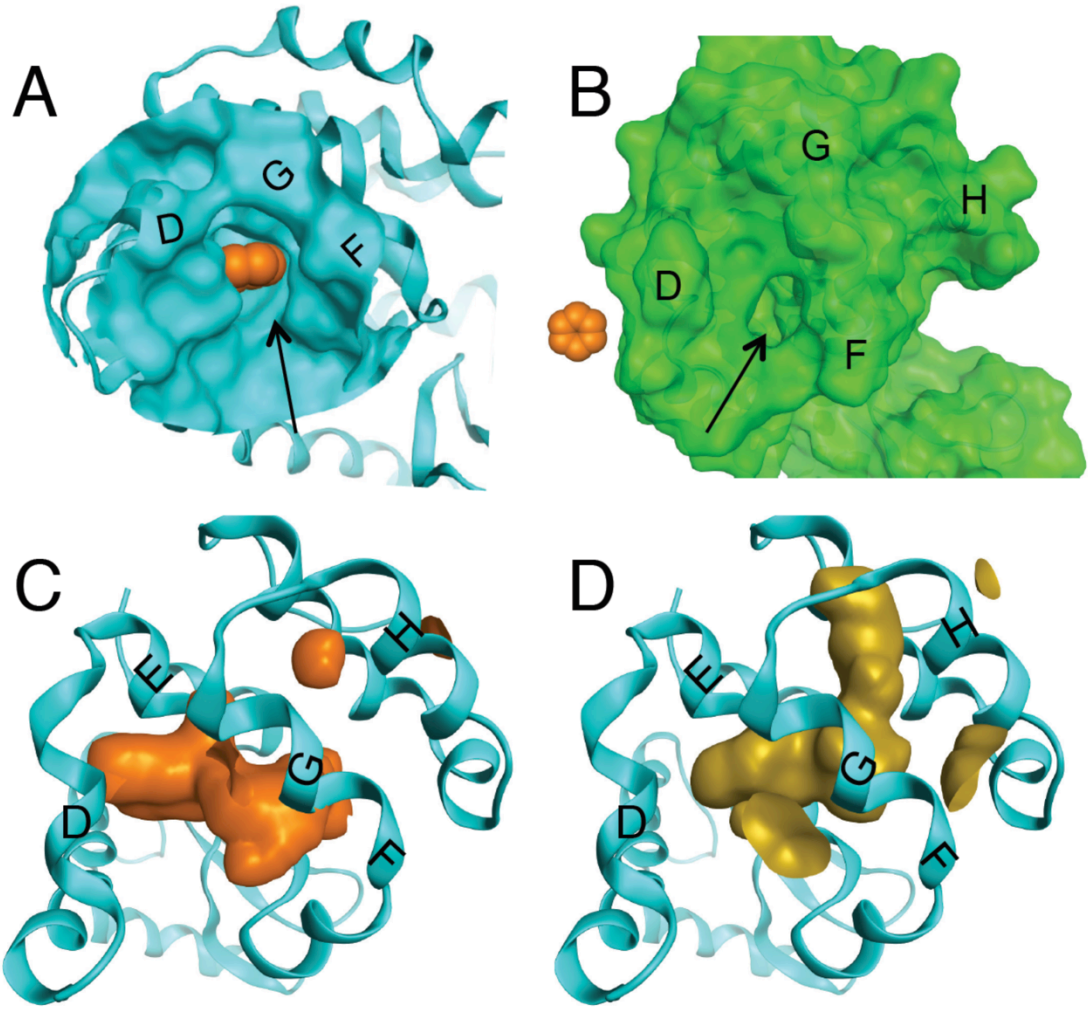

Figure S6 | Mobile defects in the ground state simulation produce multiple paths to the protein surface as potential sites of ligand egress and ingress. (A) A cavity to surface opening large enough for benzene to escape is observed between the D, F, and G helices in the holo aMD trajectory where benzene remains bound and in the apo trajectory (B), space filling representation of benzene is shown left for reference). (C, D) Mobile defects of the buried cavity in the apo trajectory reveal a number of cavity openings to surfaces. Similar potential paths have been observed previously (1-3).

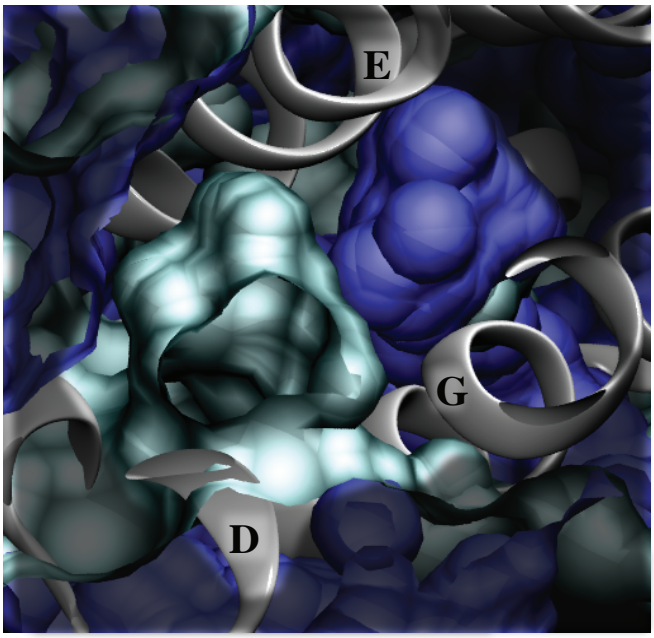

Figure S7 | Locations of the DFG and FGHI pockets differ in the C-terminal domain. In white cartoon is showing the backbone of the C-terminal domain from the L99A structure with the FGHI pocket. The FGHI pocket surface is shown in blue, where as the DFG pocket surface is shown in cyan. Snapshots from trajectory are aligned to the backbone of residues 75 to 155.

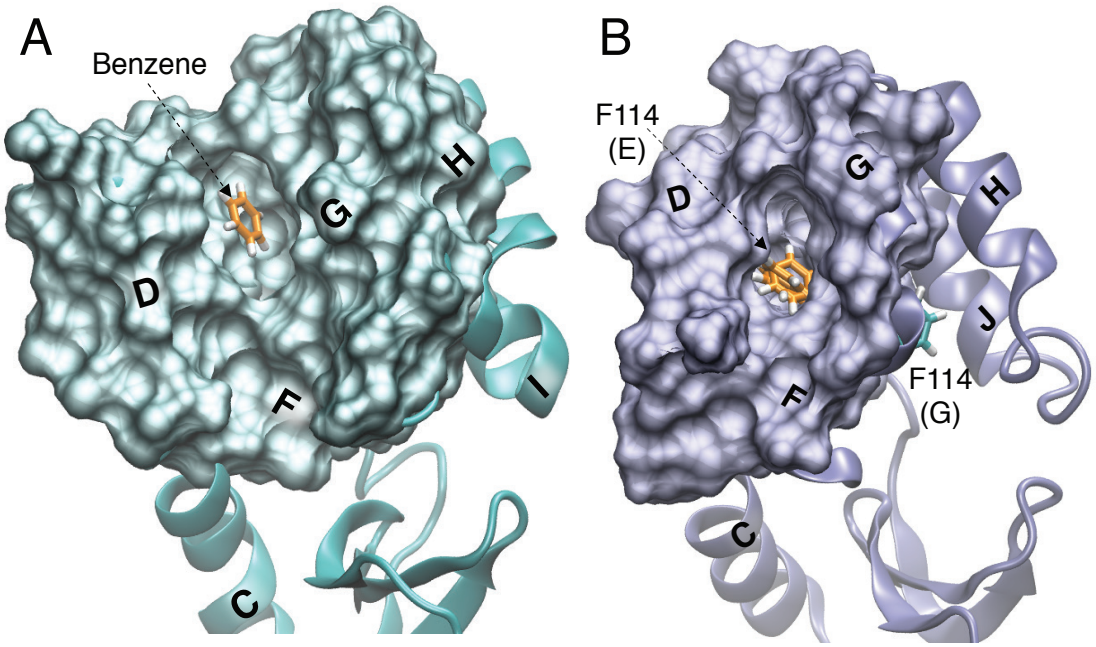

Figure S8 | A large transient packing defect precedes correlated fluctuations that allow for benzene egress and excited state transitioning. (A) The structure of L99A (holo) aMD simulation after ~ 24000 timesteps (~ 150 ns). This large cavity opening precedes the shift of benzene from S1 (ground state) to S2 substate. The surface of the protein surrounding benzene in this state consists primarily of hydrophobic sidechains. The location of benzene is shown in orange. (B) For comparison a snapshot of the L99A (apo) Anton trajectory at ~ 18 μs, just before the transition to an intermediate state that is characterized by flipping of the F114 phenyl ring into the buried cavity (Schiffer J.M. et al.). A few examples of F114 in the excited state, orange, and one example of F114 in the ground state, cyan, are shown.

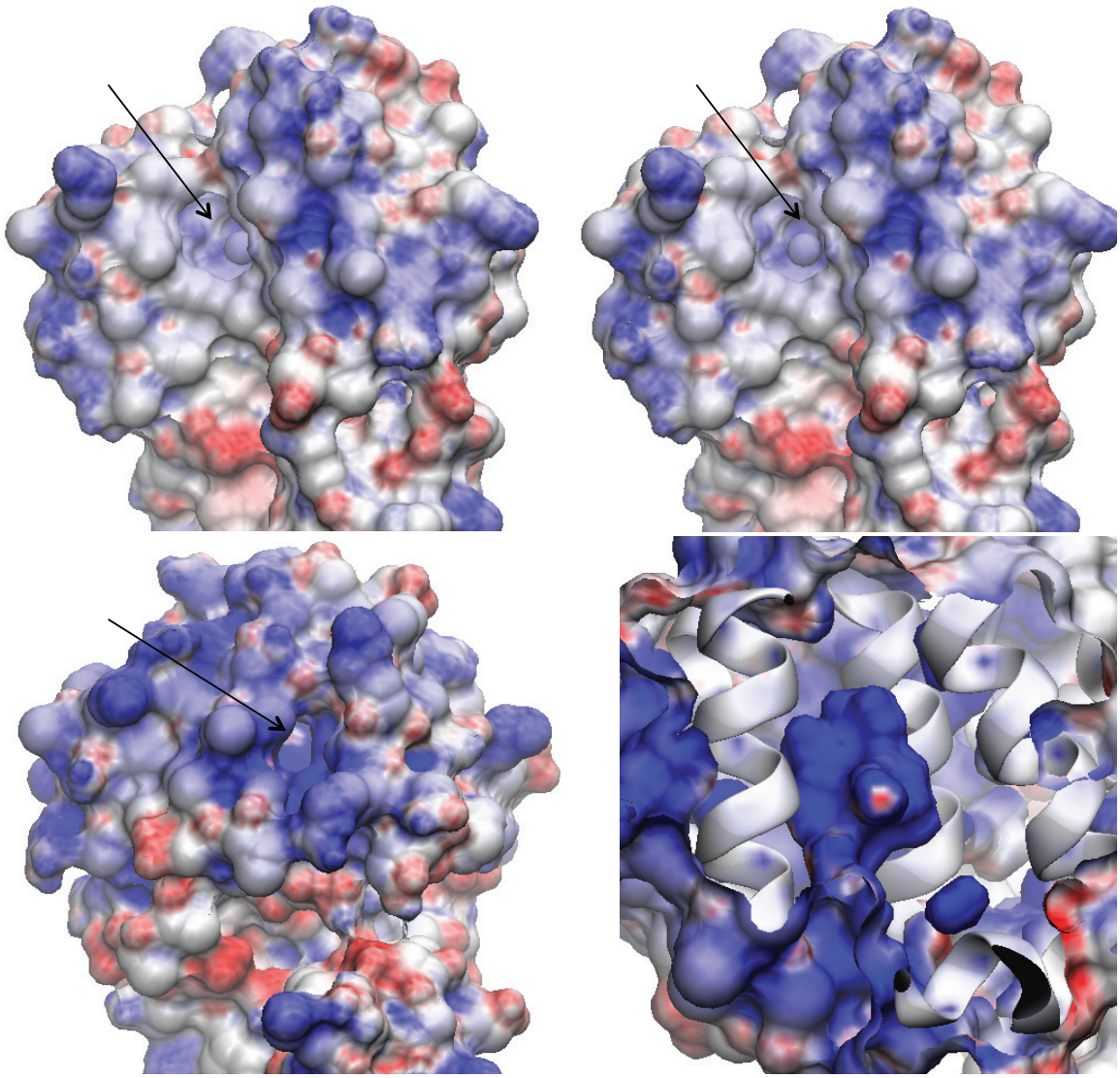

Figure S9 | Electrostatic surface maps illustrate differences between the surface openings formed by the D/G helices and the F/G/H helices. Positively charged surfaces are displayed in blue, negatively charged surfaces are displayed in red, and hydrophobic surfaces are shown in white. The cleft between the D/G helices (top) is largely nonpolar and hydrophobic, whereas the cleft formed between the F/G/H helices (bottom) is highly cationic and surrounded by charge surfaces on the solvent face.

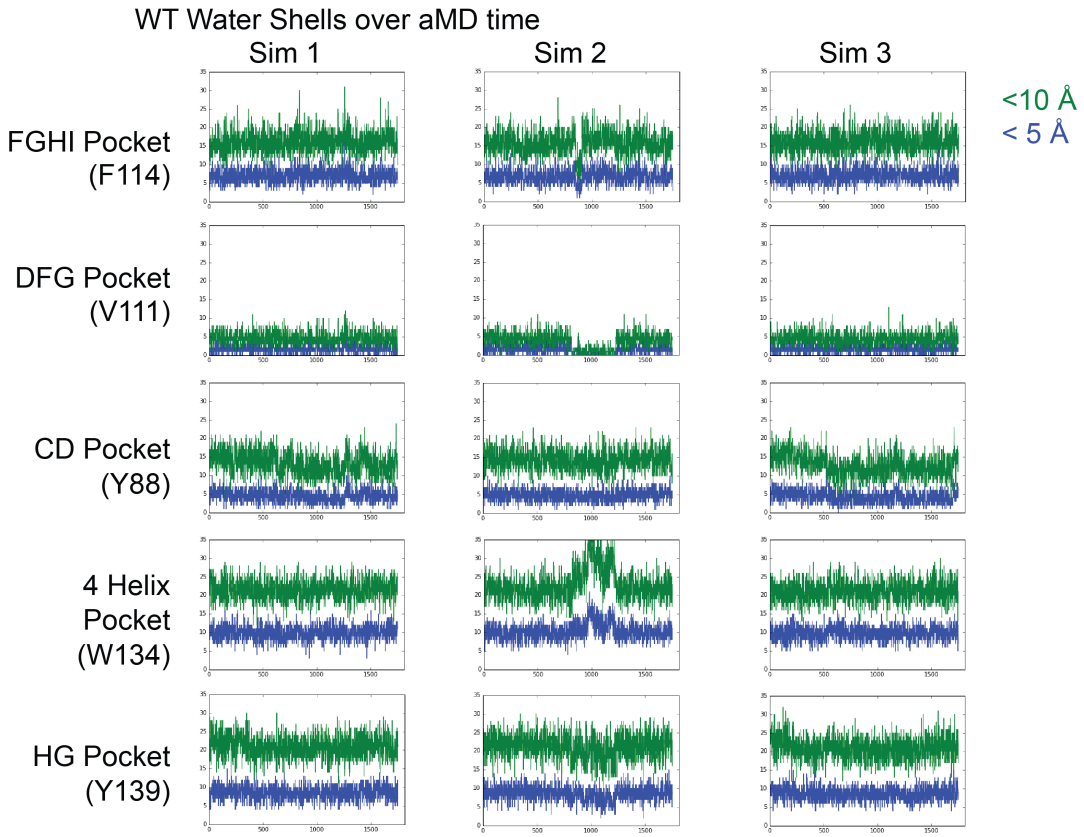

Figure S10 | Number of Waters in Watershells Around the C-terminal Domain Pockets in the WT Simulations. Each of the three replicates of the WT* simulations are shown in the columns above. The different pockets are shown in rows. The number of waters in the first water shell are shown in blue, while the number of waters in the second watershell are shown in green. The y-axis in all the plots spans from 0 waters to 35 waters. The x-axis shows the timestep of each 500 ns replicate.

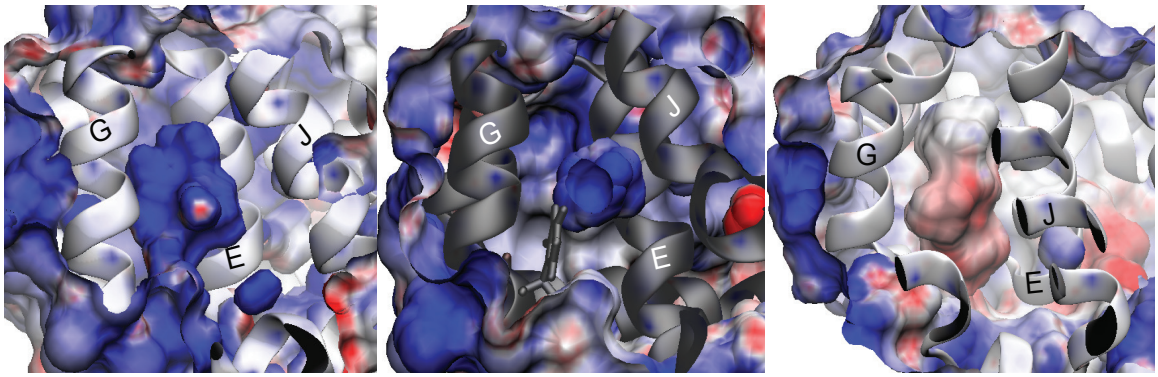

L99A BNZ leaving state aMD

WT T4 lysozyme aMD processive state

L99G T4 lysozyme Crystal

Figure S11 | Cavity polarity differences between the benzene leaving state in the L99A aMD trajectory, the processive state in the WT aMD trajectory, and the L99G T4 lysozyme crystal structure. Positively charged surfaces are displayed in blue, negatively charged surfaces are displayed in red, and hydrophobic surfaces are shown in white. The backbone secondary structures are depicted in white ribbons for mutants and black ribbon for wildtype. The L99G crystal structure has pdb code = 1QUD (4).

Supporting References:

1. Schiffer, J.M., V.A. Feher, R.D. Malmstrom, R. Sida, and R.E. Amaro. 2016. Capturing invisible motions in the transition from ground to rare excited states of T4 lysozyme L99A. Biophys. J. 111: 1-10.

2. Kitahara, R., Y. Yoshimura, M. Xue, T. Kameda, and F.A.A. Mulder. 2016.

Detecting O2 binding sites in protein cavities. Sci. Rep. 6: 20534.

3. Nunes-Alves, A., D.M. Zuckerman, and G.M. Arantes. 2018. Escape of a small molecule from inside T4 lysozyme by multiple pathways. Biophys. J. 114: 1058-1066.

4. Wray, J.W., W.A. Baase,J.D. Lindstrom, L.H. Weaver, A.R. Poteete, and B.W. Matthews. 1999. Structural analysis of a non-continguous second-site revertant in T4 lysozyme shows that increasing the rigidity of a protein can enhance its stability. J. Mol. Biol, 292: 1111-1120.

.